



HAL
open science

A scaling analysis for turbulent shock-wave/boundary-layer interactions

L. J. Souverein, P. G. Bakker, P. Dupont

► **To cite this version:**

L. J. Souverein, P. G. Bakker, P. Dupont. A scaling analysis for turbulent shock-wave/boundary-layer interactions. *Journal of Fluid Mechanics*, 2013, 714, pp.505-535. 10.1017/jfm.2012.495 . hal-03763427

HAL Id: hal-03763427

<https://hal.science/hal-03763427v1>

Submitted on 29 Aug 2022

HAL is a multi-disciplinary open access archive for the deposit and dissemination of scientific research documents, whether they are published or not. The documents may come from teaching and research institutions in France or abroad, or from public or private research centers.

L'archive ouverte pluridisciplinaire **HAL**, est destinée au dépôt et à la diffusion de documents scientifiques de niveau recherche, publiés ou non, émanant des établissements d'enseignement et de recherche français ou étrangers, des laboratoires publics ou privés.

A scaling analysis for turbulent shock wave boundary layer interactions

L.J. SOUVEREIN¹ P.G. BAKKER² AND P. DUPONT³

¹Astrium GmbH Space Transportation, Propulsion & Equipment - Advanced Programmes, Engineering & Technology, 81663 Munich, Germany

²Faculty of Aerospace Engineering, Delft University of Technology, Kluyverweg 1, 2629 HS, Delft, The Netherlands

³Institut Universitaire des Systèmes Thermiques Industriels
Aix-Marseille Université and UMR CNRS 7343, Marseille 13013, France

(Received ?? and in revised form ??)

A model based on mass conservation properties is developed for shock wave boundary layer interactions (SWBLIs), aimed at reconciling the observed great diversity in flow organization documented in literature, induced by variations in interaction geometry and aerodynamic conditions. It is the basis for a scaling approach for the interaction length that is valid independent of the geometry of the flow (considering compression corners and incident reflecting shock interactions). As part of the analysis, a scaling argument is proposed for the imposed pressure jump that depends principally on the free-stream Mach number and the flow deflection angle. Its interpretation as a separation criterion leads to a successful classification of the separation states for turbulent SWBLIs (attached, incipient or separated). In addition, dependencies of the interaction length on the Reynolds number and the Mach numbers are accounted for. A large compilation of available data provides support for the validity of the model. Some general properties on the state of the flow are derived, independently of the geometry of the flow and for a wide range of Mach numbers and Reynolds numbers.

1. Introduction

Shock Wave Boundary Layer Interactions (SWBLI) have been widely studied in the last decades (see for example the following review papers: Détery & Marvin (1986); Viswanath (1988); Dolling (2001); Smits & Dussauge (2006); Clemens & Narayanaswamy (2009); Détery & Dussauge (2009)). The most commonly considered interactions concern those with a turbulent boundary layer, although laminar or transitional interactions have also been investigated in literature. Cases under consideration covered a large range of geometric configurations (amongst others *normal shock interactions* (Atkin & Squire (1992); Bruce & Babinsky (2008); Bur *et al.* (2008)), *blunt fin interactions* (Brusniak & Dolling (1994); Ünalms & Dolling (1996); Bueno (2006)), *over-expanded nozzles* (Frey & Hagemann (1998, 2000); Bourgoing & Reijasse (2005)), *compression ramp interactions* (Thomke & Roshko (1969); Spaid & Frishett (1972); Settles *et al.* (1979); Debiève (1983); Ardonceau (1984); Dolling & Or (1985); Smits & Muck (1987); Kuntz *et al.* (1987); Selig *et al.* (1989); Erengil & Dolling (1991*a,b*); Thomas *et al.* (1994); Beresh *et al.* (2002); Hou (2003); Ganapathisubramani *et al.* (2007*a*); Wu & Martin (2008); Ringuette *et al.* (2008)) and *incident reflecting shock interactions* (Green (1970); Dupont *et al.* (2006); Pirozzoli & Grasso (2006); Touber & Sandham (2008); Piponniau *et al.* (2009); Humble

et al. (2009a); Souverein *et al.* (2009); Polivanov *et al.* (2009); Garnier (2009); Touber & Sandham (2009a); Pirozzoli *et al.* (2009); Souverein *et al.* (2010); Souverein (2010)); the list is evidently not exhaustive). In addition, the considered flow conditions cover a large range of Mach numbers (from transonic to hypersonic values) and of Reynolds numbers (spanning at least two orders of magnitude depending on the experimental facilities).

Despite these large variations in aerodynamic and geometric parameters, several general properties have been highlighted for this family of flows. The qualitative mean organization of the flow is currently quite well understood, see Détery & Marvin (1986). Good quantitative agreement has been obtained in the particular case where the shock strength is large enough for the boundary layer to separate. In those cases, the free interaction theory proposed by Chapman *et al.* (1957), suggests that the separation shock properties become independent of the original cause of the separation (i.e. the flow deflection angle). Therefore, notwithstanding the difference in flow geometry, the wall pressure distributions for sufficiently separated shock reflections and compression ramps are nearly coincident (see Détery & Marvin (1986)). However, no satisfactory description has yet been found that relates the extent of the interaction to the combined effect of variations in the Mach number, the Reynolds number, the state of the incoming boundary layer (including non-adiabatic wall conditions and upstream control) and the imposed adverse pressure gradient. Results are even worse when the geometry is also included as a parameter.

More recently, evidence of low frequency unsteadiness of the separation shock has been reported (Dolling & Murphy (1983); Dolling & Brusniak (1989); Erengil & Dolling (1991b); Thomas *et al.* (1994)). These frequencies are about two orders of magnitude below the energetic scales of the upstream boundary layer and their origin has been a subject of studies for nearly two decades.

Although the precise sources of the separation shock motions are still under debate, it has been shown recently that in separated cases, the low frequency unsteadiness of the separation shock is also rather independent of the particular geometry of the flow (Dussauge *et al.* (2006); Dupont *et al.* (2006); Wu & Martin (2008); Touber & Sandham (2009b)). For example, a dimensionless frequency of the separation shock oscillations can be defined with a nearly constant value, whatever the particular shock induced separation that is considered (see Erengil & Dolling (1991b); Dussauge *et al.* (2006)). This dimensionless frequency, or Strouhal number, is defined as:

$$S_L = \frac{fL}{U_1} \quad (1.1)$$

where f is the characteristic shock motion frequency, L the characteristic length of the interaction and U_1 the velocity downstream the separated shock. The Strouhal number S_L , originally proposed for a Mach 3 compression ramp case (Erengil & Dolling (1991b)), is similar to its counterpart for incompressible separated flows (Kiya & Sasaki (1983); Cherry *et al.* (1984)). Typical values of 0.12 are obtained in subsonic separated flows, compared to the nearly constant value of about 0.03 for supersonic cases at a Mach number larger than 2.

The characteristic length L used in the Strouhal number represents the effects of the presence of the boundary layer in comparison to a purely inviscid flow (see the scheme in figure 1). It is defined as the observed upstream shift of the shock wave C_S due to the thickening of the boundary layer, subject to the imposed pressure jump (or equivalently the angle of deviation of the flow). When the boundary layer is sufficiently decelerated to separate, the shock wave C_S is called the *separation shock*. For simplicity, we will keep this nomenclature for this shock wave, whatever the separation state of the flow.

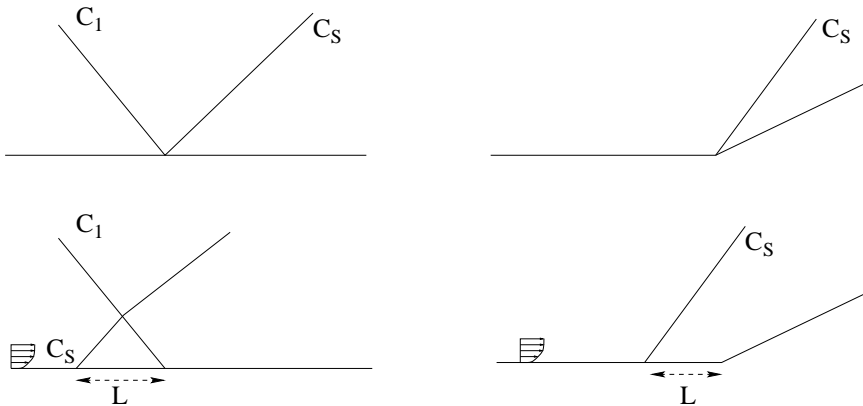


FIGURE 1. Definition of the interaction length L for reflection and compression ramp cases.

Hence, in the case of reflecting waves, L is defined as the distance between the foot of the separation shock and the extrapolated wall impact point of the incident shock. Similarly, in cases of for example compression corners and blunt fins, L is defined as the distance between the foot of the separation shock and the corner, respectively the obstacle. It has to be noted that the derivation of the location of the foot of the separation shock can differ depending on the authors and the published data. It has sometimes been derived from Schlieren visualizations, from particle image velocimetry data, from the mean wall pressure distribution, or it is associated with the peak in the wall pressure fluctuations, p'_w . This, of course, will introduce some discrepancies in the estimation of L . It will however be shown that these are significantly less than the observed aerodynamic and geometrical effects. In cases with large separation, L can be considered as a rough estimate of the length of separation L_{sep} which is poorly documented in literature.

Several attempts have been made to relate the low frequency shock motions to upstream or downstream unsteadiness. In high Reynolds compression corner or shock reflection configurations ($Re_\theta \simeq 5 \times 10^4$, where Re_θ is the Reynolds number of the upstream boundary layer based on the momentum thickness), several experimental studies suggested to relate the separation shock motions to unsteady very large structures developed in the upstream boundary layer (Ganapathisubramani *et al.* (2007a); Humble *et al.* (2009a)). On the contrary, experimental and numerical studies performed at low Reynolds ($Re_\theta \simeq 5 \times 10^3$) indicate that the low frequency shock motions are related to the dynamics of the separated bubble which forms downstream of the separation shock (Dupont *et al.* (2006); Toubert & Sandham (2008); Wu & Martin (2008); Piponniau *et al.* (2009)).

Recently a simple model has been proposed relating the value of the Strouhal number to the entrainment properties of the mixing layer which develops over this separated region (Piponniau *et al.* (2009)). This model suggest a major influence of the compressibility effects on the decrease of this Strouhal number from its subsonic value (≈ 0.12) to its asymptotic value (≈ 0.03) for free stream Mach numbers larger than 2. Taking into account these compressibility effects and the classical effects of the velocity and density ratios across the mixing layer, this model successfully describes the behavior of the Strouhal number for a large number of separated flows, ranging from subsonic to hypersonic flows, and for a wide range of Reynolds numbers. Other works propose to consider the whole interaction as a dynamic system with its own transfer function. Initially suggested in Plotkin (1975), this approach has been recently re-considered in the case of a Mach 2.3 shock reflection in Toubert & Sandham (2011), where the interaction is proposed

to act as a low pass filter for the upstream perturbations. This analysis, based on the similitude properties of the flow inside the first part of the interaction, estimated with success the characteristic time scale of shock unsteadiness in the IUSTI (Institut Universitaire des Systèmes Thermiques Industriels) 8° interaction. These two models differ mainly on the nature of the low frequency unsteadiness: Touber & Sandham's model suggests a broad band mechanism without a particular time scale, limited by the equivalent cut-off frequency of the system. On the contrary, the model of Piponnier *et al* suggests the existence of a characteristic frequency, eventually with some time fluctuations, due to the turbulence and/or some harmonics in the entrainment time scales. Both types of unsteadiness could even cohabit, as suggested in Touber & Sandham (2011).

In these two last models, the basic driving mechanism for the unsteadiness is derived from the analysis of the mixing layer which is observed downstream the separation point in all flows with shock induced mean separation. The model of Piponnier *et al* considers the entrainment influence of the mixing layer whereas the model of Touber & Sandham is based on its similarity properties. Nevertheless, the mechanisms driving the unsteadiness in the case without mean separation are not intuitively evident. Recent experiments on incipiently separated shock reflection interactions were carried out in the low Reynolds supersonic wind tunnel of the IUSTI and in the high Reynolds number one of the TU Delft (Souverein *et al.* (2009, 2010)) to shed light on this issue. A large Reynolds number range has been considered ($4000 < Re_\theta < 50000$). In these cases, no mean separation is obtained, but instantaneous reverse flow regions can be observed. These experiments show that incipient cases display large similarities and that the Reynolds number effects on the global properties of the interaction are rather limited. For example, a large resemblance was found in the turbulent fields. Moreover, in both incipient cases, evidence of the development of a mixing layer region downstream the reflected shock has been given, with a spatial development that resembles the separated cases, with indications for the existence of low frequency shock motions. However, notwithstanding the presence of the mixing layer, unsteadiness in the upstream boundary layer was also shown to play a role in flows without mean separation.

Despite the successful scaling of the low frequencies unsteadiness based on the characteristic length L , no satisfactory scaling of L itself has been derived so far for turbulent SWBLIs. For example, despite a similar geometry, no direct comparison of the length of the interactions could be made for the two reflection cases with incipient separation previously mentioned. It will be shown that this is even worse when different geometries are considered.

Given the discussion above, it seems desirable to obtain a better description of the characteristic length L , both for the quantitative comparison of different interaction geometries under varying flow conditions, and due to its role as a scaling parameter for the low frequency unsteadiness. In this article, it is proposed to compare the characteristic length scales of shock wave boundary layer interactions for various flow conditions and separation states. Of particular interest is the dependence of the characteristic length on the upstream boundary layer and the imposed pressure jump. A simple analysis is made based on a global mass budget along the interaction to derive the parametric dependencies for this sort of flows, whatever the geometric conditions (compression corner, incident shock wave....) and Mach and Reynolds number. The model will be presented in section 2, and then compared with experimental and numerical results obtained for a wide range of Mach and Reynolds numbers, for compression corners and incident shock reflections. The parametric dependence will be discussed and verified against the data available in the literature in section 3. Finally, the possibility of using the new length scaling for the analysis of turbulence fields will be considered in two oblique shock wave / turbulent

boundary layer interactions. The first interaction concerns the low Reynolds number, Mach 2.3 flow case of the IUSTI and the second one the large Reynolds number, Mach 1.7 flow case of the TU Delft.

2. Scaling arguments for shock wave boundary layer interactions

2.1. Length of interactions in various SWBLIs

Shock wave boundary layer interactions (SWBLIs) present large qualitative similarities whatever the aerodynamic and geometric parameters. Nevertheless, despite their large resemblance and the successful scaling of the unsteadiness time scales based on the Strouhal number, it remains quite difficult to compare the length scales of these interactions. Several scaling approaches have been attempted for the interaction length L and the shock intensity Δp . An example is given in figure 2. It proposes that $\frac{L}{\delta^*} \sim \frac{\Delta p}{\tau_w}$, where δ^* is the displacement thickness of the upstream boundary layer and τ_w the wall shear stress: a reasoning that finds its origins in the Free-Interaction concept, see Détery & Marvin (1986). The figure encompasses two flow cases (reflecting shock interactions and compression ramp interactions) for a wide range of flow conditions (Mach number, Reynolds number, flow deflection angle) and flow facilities. Direct Numerical Simulation and Large Eddy Simulations are also included. Finally, the state of the interaction, when documented, is used to define the color of the symbol: black for attached flows, gray for incipient and white for separated ones. Cases where the separation state is unknown, or where uncertainty exists concerning its determination, are indicated with closed symbols (e.g. the asterisks). Some points of interest have been highlighted to illustrate the data range covered by the figure. To be able to compare the ramp flow and reflected shock cases, the pressure rise is defined over the complete interaction. The literature sources and the short names used in this and all subsequent figures are summarised in tables 1 and 3. It is noted that the interaction geometry is included as a parameter, since it is believed that the relation between the pressure jump and the interaction length should be properly captured, independent of the particular geometry imposing the pressure jump. This seems to be a reasonable point of view, given the previously recalled observations in literature (notably the Free-Interaction concept) that notwithstanding the difference in flow geometry, the wall pressure distributions are nearly coincident, at least in the case of compression ramps and incident shock reflections.

The scaling collapses shock reflection data from the IUSTI S8-facility and data from a similar facility at ONERA taken under close measurement conditions. Both also incorporate the effect of a heated wall, with $T_w/T_{aw} = 2$, where T_w and T_{aw} are respectively the heated wall and the adiabatic wall temperature (see Laurent (1996), Benkemoun & Salaun (1988)). The resulting curve shows a monotonically increasing dependence between L and ΔP .

The data overview shown in figure 2 is subject to the accuracy of several flow parameters, where the principal uncertainty is expected in the determination of the length scales and the boundary layer state: the upstream displacement thickness δ^* , the wall friction τ_w and the length of interaction L (it is supposed that the the free stream Mach number and the flow deflection angle are setting parameters that are known with sufficient accuracy). For example, the University of Princeton high Reynolds ramp flow (excluding the Settles *et al.* (1976) data) exhibit variations in the specified incoming boundary layer properties from one reference to the other. As stated by Selig *et al.* (1989), these variations do not correspond to physically different boundary layer states, but are due to differences in definitions and determination methods. The scatter in the reported values

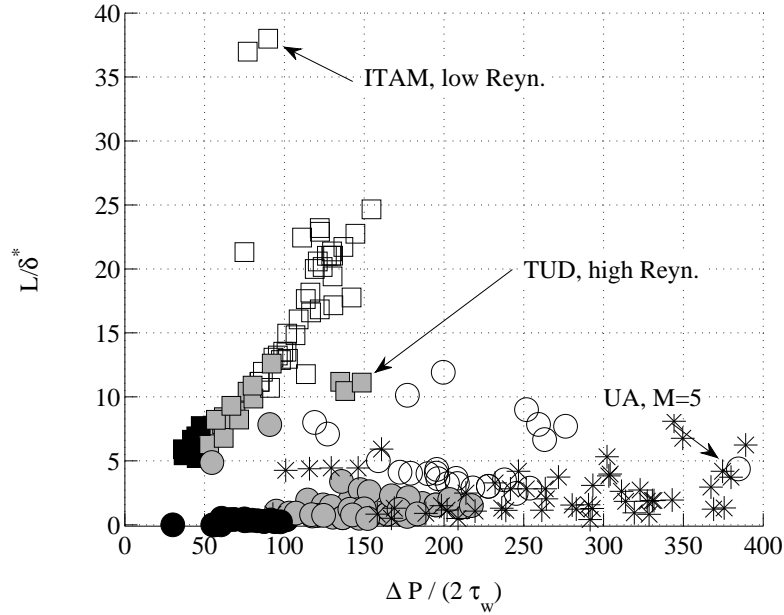


FIGURE 2. Scaling: $\frac{L}{\delta^*}$ vs. $\frac{\Delta p}{2\tau_w}$. \square : incident shock reflections; \circ : compression ramps. See references in table 1 on page 7 and table 3 on page 20 for a complete list of the included data sets. Colours represent the separation state (black: attached; grey: incipient; white: separated).

of δ^* amounts to $\pm 15\%$. The uncertainty in the determination of the interaction length is reasonably no less than 5%. In addition, the interaction length for attached flows is non-zero, even though the separation length vanishes: in compression ramp cases, where L is often derived from the separation point, an offset near 0 will hence appear. Given these uncertainties and the wide range of measurement techniques, it should therefore be expected that any attempt to collapse data onto a single curve will be faced with an experimental disparity that could amount up to $\pm 20\%$.

Nevertheless, considering interactions with the same separation state (attached / separated), the values of $\frac{L}{\delta^*}$ and $\frac{\Delta p}{2\tau_w}$ show a disparity amounting up to 500%. Moreover, it is remarked that there is a general Reynolds number trend in the figures from top left (low Reynolds cases) towards bottom right (high Reynolds cases). In addition, there seems to be a Mach number dependence, with the highest Mach number cases located towards the extreme right. The scaling clearly does not correctly take into account the Reynolds number effects, the Mach number effects and the different interaction geometries (incident reflecting shock and compression ramp). It is noted that comparable results are obtained when scaling L with the upstream boundary layer thickness δ_0 , an approach that was applied with some success in Dupont *et al.* (2006).

Given the above results it is concluded that there exists a dependence between the interaction length L and the shock intensity Δp , but that the scaling with respectively δ_0 or δ^* and τ_w is not satisfactory. Data taken under the same reference conditions do indeed collapse onto a single curve, but the scaling breaks down when changing the Mach number, the Reynolds number or the interaction geometry.

This might indicate that the physical cause for the upstream displacement of the reflected shock is not properly captured, and that the origin of this displacement is not

TABLE 1. Interactions considered in subsequent figures.

Short	Institute	Literature
<i>Incident shock reflections</i>		
IUSTI	IUSTI, Marseille	Laurent (1996), Dupont <i>et al.</i> (2006), Piponniau <i>et al.</i> (2009), Piponniau (2009), Souverein <i>et al.</i> (2010), Souverein & Debiève (2010), Souverein (2010)
<i>Compression ramps</i>		
UP	University of Princeton	Settles <i>et al.</i> (1979), Dolling & Or (1985), Selig <i>et al.</i> (1989), Settles <i>et al.</i> (1976)
UND	University of Notre Dame	Thomas <i>et al.</i> (1994)
UI	University of Illinois	Kuntz <i>et al.</i> (1987)
<i>Incident shock reflections:</i>		
∇ IUSTI: $Re_\theta = 5.0 \times 10^3$, $M_e = 2.3$		
<i>Compressions ramps:</i>		
◇ ,UND: $Re_\theta = 17.5 \times 10^3$, $M_e = 1.5$		
△, UI: $Re_\theta = 21 \times 10^3$, $M_e = 2.9$		
★ UP: $Re_\theta = 70 \times 10^3$, $M_e = 2.9$		
○ UP: $Re_\theta = 18 - 300 \times 10^3$, $M_e = 2.3$, Settles		

limited to an upstream reference scale. Redefining only one of the axes in figure 2 cannot make the curves collapse in a way that makes physical sense: only redefining the scaling for either Δp or L may make all data collapse, but in the best case, the most separated compression ramp interactions will collapse with the attached incident reflecting shock cases. A new scaling must therefore be defined for both Δp and L : this is the core of the present work.

As a starting point, it is assumed that L is some function F_1 of the reference flow conditions, see equation 2.1.

$$L = F_1(M_e, Re_\theta, \varphi, \frac{T_w}{T_{aw}}, \text{geometry}, \dots) \quad (2.1)$$

where φ is the flow deviation (the corner angle for compression ramps and the deviation angle across the incident shock in flow reflection cases).

It is now attempted to reformulate the expression in equation 2.1 in such a way as to obtain a relation between a non-dimensional interaction length (L^*) and a non-dimensional interaction strength parameter that represents the tendency of the flow to separate (S^*), in other words:

$$L^* = F_2(S^*) \quad (2.2)$$

where F_2 is a still to be defined function. It is proposed to define the non-dimensional interaction strength parameter S^* as:

$$S^* = \frac{\Delta P}{\Delta P_{sep}} \quad (2.3)$$

where ΔP_{sep} is the shock intensity needed to make the boundary layer to separate. It was shown in the previous section that an evaluation of the separation criteria based on the viscous scales of the boundary layer failed to classify the different interactions.

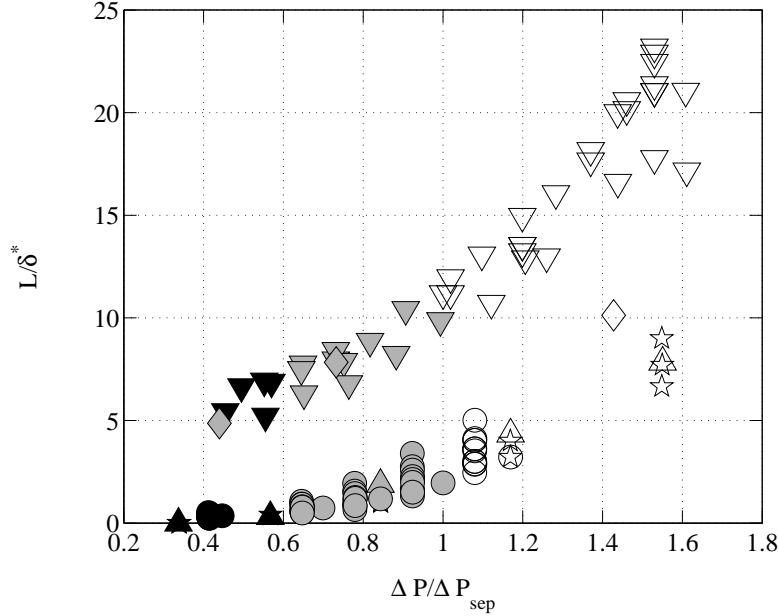


FIGURE 3. Scaling: $\frac{L}{\delta^*}$ vs. $\frac{\Delta P}{\Delta P_{sep}}$. Symbols according to table 1 on page 7.

Consequently, the difficulty is: how to define the shock intensity ΔP_{sep} for the different interactions presented in the previous section. For the numerical simulations often only a single flow deviation angle is considered, with a focus on separated cases; no information on the onset of flow separation is available. Similarly, in several experimental works, only one flow deviation is considered. Therefore, for the moment, only experiments will be taken into account where several flow deviations have been considered (covering all cases from attached to separated conditions) and where the separation state has been determined. This enables the direct evaluation of the separation criteria S^* defined by 2.3. The result is illustrated in figure 3, with corresponding references given in Table 1.

It is clear that, notwithstanding the fact that the different interactions are now classified according to their separation state, no satisfying collapse has been obtained for the two geometries: shock reflection and compression corner: the reflection case exhibits a non-dimensional length of about 2 to 4 times larger than the compression corner for equivalent separation states. Moreover, apart from the limited (low) Reynolds number range covered by the subset of shock reflection interactions shown in figure 3, all data has been obtained at a Mach number of 2.3; hence, a certain effectiveness of the data collapse for this geometry case should come as no surprise. Things are different for the subset of compression corner experiments, which cover a wider range of Mach numbers (from 2 to 5) and Reynolds numbers (from 2×10^3 to 3×10^5), although for this geometry case most of the experiments were performed at Mach numbers in close vicinity of 3. Nevertheless, the experiments from UND clearly diverge from the general trend: these experiments involve lower Mach numbers ($M = 1.5$), suggesting that both the geometry and the Mach number have to be involved in the derivation of L^* .

In the sections below, it will therefore be attempted to define a more suitable scaling for the interaction length that represents the relation between L and the change in boundary layer state induced by Δp for use as L^* in equation 2.2. This will be done by considering

the integral form of the mass and momentum balance for two interaction cases (incident reflecting shock and compression ramp). The new scaling will then be formalised by verifying whether it makes all data fall onto a single curve when plotted against $\frac{\Delta p}{\Delta P_{sep}}$, representing relation 2.2. Finally, the possibility to derive an efficient separation state criteria will be considered in section 2.3 and the analysis will be extended to the whole set of data, including the numerical results.

2.2. Interaction length scaling

Several investigations have been performed concerning the Mach and Reynolds number effects on the interaction length (see for example Thomke & Roshko (1969); Spaid & Frishett (1972); Settles *et al.* (1976)), putting in evidence a dependence on the Reynolds number. Intuitively, it would seem that δ^* could play this role. Nevertheless, it is clear from figure 3 that scaling with δ^* alone does not succeed in collapsing the different geometric configurations, nor does it correctly take into account the Reynolds number and Mach numbers effects. It will therefore be attempted to define a more suitable scaling that represents the relation between L and the state of the boundary layer for use as L^* in equation 2.2.

2.2.1. Model definition and assumptions

To develop this reasoning further, an inviscid model is defined based on the integral form of the conservation laws. The presence of the boundary layer is taken into account through the integral of the upstream and downstream velocity and density profiles (in other words: δ^* and θ). Furthermore, it is assumed that at the exit plane, the pressure jump imposed by the shock system (Δp) equals the inviscid value, and that the fluid is parallel to the wall. One may visualise this in terms of the inviscid flow field representation mentioned in Déleroy & Marvin (1986), see figure 4, with the difference that a displacement thickness is added at the wall. The physical cause of the interaction length may now be interpreted as a change in displacement thickness between the upstream and downstream states, creating a kind of ‘equivalent’ step at the wall. In the current model, it is attempted to define a scaling that links the interaction length to the change in boundary layer state induced by the processes within the interaction resulting from the imposed pressure jump. The downstream evolution of the length scales (due to a recovery of the boundary layer and boundary layer growth) are therefore by definition not relevant to the formulation of the scaling. The model is based on a quasi-steady state assumption and only considers the mean flow. Temporal variations are for the moment not included, but could prove an interesting extension of the model.

To concretise these ideas, a control volume approach is defined, enclosing the interaction region. It is assumed that the flow is two dimensional and steady in the mean. In the formulation of the inviscid flow model, the viscous terms are inherently neglected with respect to the pressure force and the inertial terms in the deduction of the momentum conservation based formulation.

For the definition of the control volume, a thought experiment is made. It is imagined that we are looking at the interaction from far away, such that $\frac{\delta_0}{L_{cv}}, \frac{\theta_0}{H_{cv}} \rightarrow 0$, where L_{cv} and H_{cv} are the length and the height of the control volume respectively. In that case, the interaction is reduced to almost a single point and the flow is essentially the same as for the inviscid case. Now let us image that we zoom in again, putting ourselves close enough to see the complexities of the interaction, but far away enough such that the reflected shock, the expansion fan and the successive recompression waves have all coalesced to form the single shock prescribed by the inviscid flow solution. Putting ourselves in this position, we can model the interaction as a black box that modifies the state of the

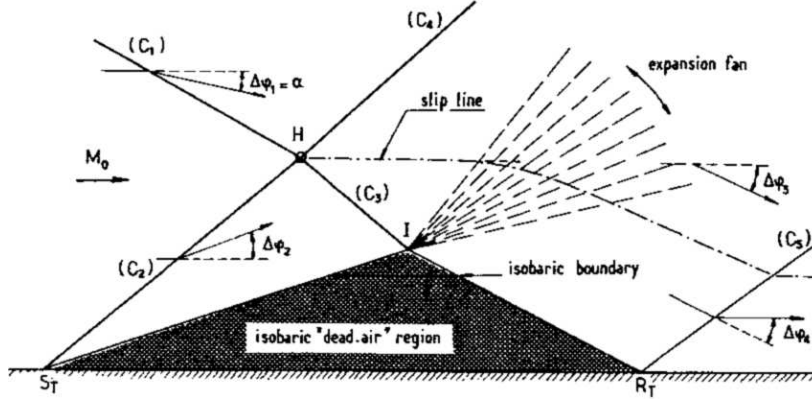


FIGURE 4. Inviscid flow model for the shock-reflection interaction with separation, from Détery & Marvin (1986).

boundary layer. The flow conditions on all sides of the control volume are prescribed by the free-stream conditions and the inviscid oblique shock relations. The presence of the boundary layer can be taken into account through the definition of the displacement thickness.

In the proposed model, the edge conditions must adhere to the inviscid shock reflection conditions. The pressure gradient imposed by the shock system will lead to a deceleration of the boundary layer and therefore to an increase of the displacement thickness through the interaction as compared with the upstream thickness. Consequently, the only way for the flow to assure mass and momentum conservation in the presence of the boundary layer is to translate the reflected shock, see figure 5(a) for the reflection case and figure 5(b) for the compression corner. This translation can be cast into an algebraic equation by considering the difference between the inviscid case (the perfect fluid solution without boundary layer and interaction) and the viscous case (with interaction, the viscous effects being modeled as discussed above).

It is reiterated that the basic assumptions are that the shock intensity is the same as in the perfect fluid flow reflection, and that at the outflow plane, the flow conditions outside the boundary layer become uniform and approach the perfect fluid solution. Indeed, in reality one is confronted with deviations from the model assumptions. One may think of the presence of the expansion fan and velocity gradients that curve the path of the shock within the control volume, inducing for instance a discrepancy between the measured shock position (by means of wall pressure distributions) and the position as defined by the model. In addition, this curving causes entropy gradients, leading to a non-homogeneous velocity and density distribution downstream of the interaction. Although the conservation laws must inherently be satisfied, difficulties are hence to be expected, particularly when modeling the outflow conditions by an integral boundary layer length scale in combination with a uniform velocity and density. All these effects will play a role when one would want to employ the model for predictive purposes. However, the current aim is to determine the most dominant mechanisms that govern the interaction length rather than to make precise length estimations. In this context, the deviations are thought to be only of secondary importance. The basic assumptions are therefore believed to be reasonable approximations for the purpose of this work.

It is remarked that both the mass balance and the momentum balance can be considered individually to derive a physical relation between the upstream and downstream boundary layer length scales and the interaction length. This has indeed been done, yield-

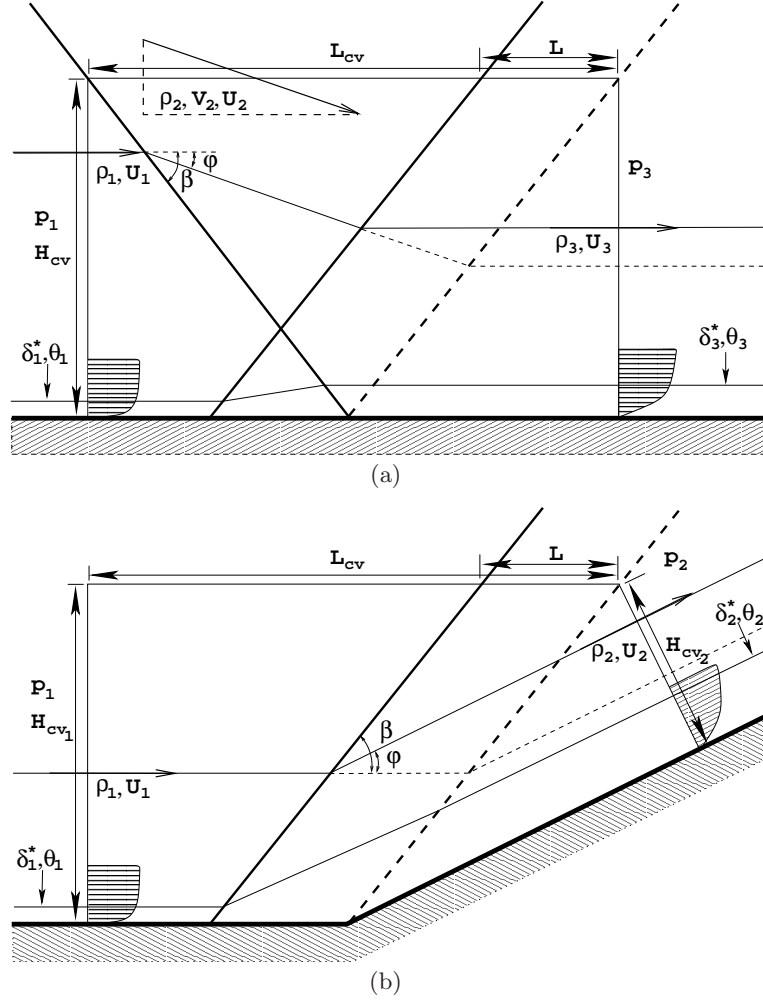


FIGURE 5. Control volume: (a) incident shock reflection case; (b) compression ramp case.

ing complementary scaling relations because both quantities must be conserved across the interaction. Since the procedure for deriving both formulations is similar, details will be given here for the mass balance only. The deduction of the momentum balance based formulation is reported in the Appendix. It is also investigated whether a commonality may be expected in the scaling for the incident reflecting shock interactions and the compression ramp flows.

Both principal geometrical cases are first considered separately: the incident shock reflection and the compression ramp. Then it will be shown that a common formulation can be derived.

Incident shock reflection

The control volume for the incident reflecting shock interaction is shown in figure 5(a). Writing the mass flow balance for the inviscid flow case (without interaction, as indicated by the dashed reflecting shock) the following equality is obtained:

$$\rho_1 U_1 H_{cv} + \rho_2 V_2 L_{cv} - \rho_3 U_3 H_{cv} = 0 \quad (2.4)$$

where H_{cv} and L_{cv} are the height and length of the control volume respectively. At the same time, the following relation is obtained for the viscous case (with interaction, as indicated by the solid reflecting shock):

$$\rho_1 U_1 (H_{cv} - \delta_1^*) + \rho_2 V_2 (L_{cv} - L) - \rho_3 U_3 (H_{cv} - \delta_3^*) = 0 \quad (2.5)$$

Subtracting equation 2.4 from 2.5, the following algebraic relation for the interaction length is obtained for the shock reflection case:

$$L = \frac{\rho_3 U_3 \delta_3^* - \rho_1 U_1 \delta_1^*}{\rho_2 V_2} \quad (2.6)$$

The interaction length is hence completely determined through the upstream and downstream boundary layer displacement thickness, since the densities and velocities are specified by oblique shock wave theory (depending only on M_e and φ). The expression is independent of the height and length of the control volume as long as the interaction is included.

Compression ramp

The compression ramp case is now considered. The control volume is shown in figure 5(b). Writing again the mass flow balance for the inviscid flow case, the following equality is obtained:

$$\rho_1 U_1 H_{cv_1} - \rho_2 U_2 H_{cv_2} = 0 \quad (2.7)$$

At the same time, the following relation is obtained for the case with interaction:

$$\rho_1 U_1 (H_{cv_1} - \delta_1^*) - \sin(\varphi) \rho_2 U_2 L - \rho_2 U_2 (H_{cv_2} - \delta_2^*) = 0 \quad (2.8)$$

Subtracting equation 2.7 from 2.8, the following algebraic relations is obtained for the interaction length for the compression ramp case:

$$L = \frac{\rho_2 U_2 \delta_2^* - \rho_1 U_1 \delta_1^*}{\sin(\varphi) \rho_2 U_2} \quad (2.9)$$

The interaction length is again completely determined through the upstream and downstream boundary layer displacement thickness, since the densities and velocities are specified by oblique shock wave theory (depending only on M_e and φ). Again, the expression is independent of the height and length of the control volume as long as the interaction is included.

2.2.2. Common formulation

Given the great resemblance between relations 2.6 and 2.9, it is tempting to see whether both equations can be cast into a common form. To this aim, the denominator of each equation is reformulated in terms of the upstream conditions by means of the oblique shock wave relations. The shock angle β and the flow deflection angle φ are defined positive for both interaction cases. Invoking mass conservation across the incident shock for the shock reflection case, the following equality is obtained:

$$\rho_1 U_1 \sin(\beta) = \rho_2 V_2 \frac{\sin(\beta - \varphi)}{\sin(\varphi)} \quad (2.10)$$

Similarly, considering mass conservation across the shock for the compression ramp case gives:

$$\rho_1 U_1 \sin(\beta) = \rho_2 U_2 \sin(\beta - \varphi) \quad (2.11)$$

Rewriting each of the equations above and substituting in their respective relations (equation 2.6 for the incident shock interaction and 2.9 for the compression corner) gives the same final equation, which can be cast into the following common form, when using the subscripts *in* and *out* for the inflow and outflow conditions respectively:

$$\frac{L}{\delta_{in}^*} = \frac{\sin(\beta - \varphi)}{\sin(\beta) \sin(\varphi)} \left(\frac{\rho_{out} U_{out} \delta_{out}^*}{\rho_{in} U_{in} \delta_{in}^*} - 1 \right) \quad (2.12)$$

The shock angle β is an algebraic relation in terms of the flow deflection angle φ and the upstream Mach number M_e . The interaction length is therefore a direct algebraic function of the M_e , φ and the mass flow deficit ratio between the incoming boundary layer and the outgoing boundary layer. Defining the mass flow deficit as $\dot{m}^* = \rho U \delta^*$ we can hence write:

$$\frac{L}{\delta_{in}^*} = g_3(M_e, \varphi) \left(\frac{\dot{m}_{out}^*}{\dot{m}_{in}^*} - 1 \right) \quad (2.13)$$

With $g_3(M_e, \varphi)$ the ratio of sine functions:

$$g_3(M_e, \varphi) = \frac{\sin(\beta - \varphi)}{\sin(\beta) \sin(\varphi)} \quad (2.14)$$

Based on this relation, it can be concluded that the interaction length is a direct result of the mass flow deficit ratio between the incoming and outgoing boundary layer, and that it can be estimated algebraically when all quantities in the equation are known.

The analysis above based on the mass conservation consideration leads to a physical insight concerning the scaling parameters for the interaction length (the vertical axis of figure 2). Relation 2.13 seems to indicate that the proper scaling of L is indeed with δ^* , but that a trigonometrical correction factor is required in the form of function g_3 . In fact, the non-dimensional interaction length represents the change of state between the incoming boundary layer and the outgoing boundary layer. It should be interpreted in terms of the mass flow deficit ratio. This explains why a simple scaling by a single boundary layer length scale did not manage to collapse the data. The proper scaling, with L^* the non-dimensional interaction length, would hence be:

$$\begin{aligned} L^* &= \frac{L}{\delta_{in}^*} G_3(M_e, \varphi) \\ &= \frac{\dot{m}_{out}^*}{\dot{m}_{in}^*} - 1 \end{aligned} \quad (2.15)$$

With:

$$G_3(M_e, \varphi) = g_3^{-1}(M_e, \varphi) = \frac{\sin(\beta) \sin(\varphi)}{\sin(\beta - \varphi)} \quad (2.16)$$

Hence, L^* becomes a function of the mass flow deficit ratio across the interaction which depends on the adverse pressure gradient imposed on the upstream boundary layer, independently of the geometry and the upstream boundary layer scales. In order to formalise this dependence between L^* and the (non-dimensional) pressure gradient S^* , L^* should therefore classify the different states of the interaction, from attached to separated cases. As a verification, both scaling options, the original $\frac{L}{\delta^*}$ and the new scaling L^* defined by equation 2.15, are compared by plotting them against the documented

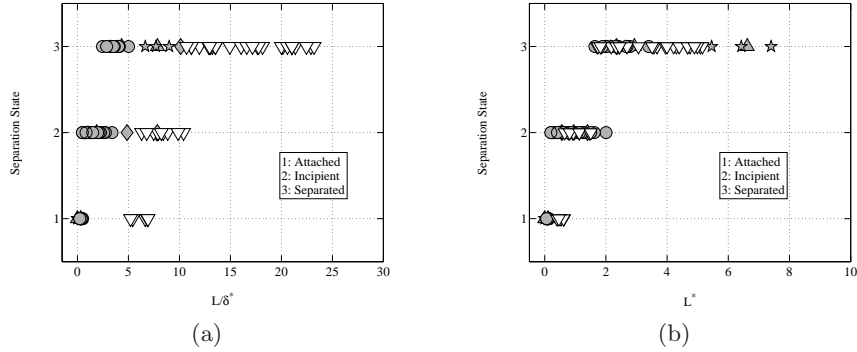


FIGURE 6. Interaction length scaling and documented separation states of the reference interactions: (a) original scaling with δ^* ; (b) new scaling based on mass conservation. Symbols according to table 1 on page 7, colours represent the two flow geometries (white: shock reflection; grey: compression ramp).

separation state, as was done for the separation criterion in the previous section. The result is shown in figure 6, with symbols corresponding to table 1 and colours representing the two interaction cases (white: incident reflecting shock; grey: compression ramp). It is clear that the first choice does not classify the flows. Moreover, the results are largely dependent on the geometry of the flow: shock reflections produce significantly larger interactions whatever the separation state of the flow. On the contrary, the new scaling leads to a better classification of the known separation states, and there is a larger consistency between the ramp flow cases and the shock reflection cases, since data corresponding to both geometries are no longer clearly distinct. The attached flow cases take on the value close to zero, as is to be expected from the definition of the scaling: the interaction length becomes small and consequently, the mass flow deficit is only slightly altered. It is noted that due to the previously mentioned limitations of the compilation concerning the determination of L , a value of $L \equiv 0$ is obtained for some of the attached interactions. Particularly for compression ramp interactions the obtained value of L depends strongly on the measurement technique and resolution for (almost) attached flows, and therefore the interaction length vanishes for small flow deflections. This is not true strictly speaking, however L will be very small and hence the attached flow cases will indeed approach $L^* \downarrow 0$, with a value identical to zero for vanishing shock intensity. The incipient interactions have a non-dimensional interaction length with a value centered around one. The separated interactions take on a value larger than two. These properties are summarised in table 2. Therefore, the proposed scaling seems efficient to compare the characteristic length scales of the interactions.

The new scaling for L is put to the test in figure 7. The same symbols are used as in figure 3. The data fall onto a single trend line. In addition, there is a classification of separation states along the curve (attached, incipient, separated), with a progressive increase in the extent of flow separation when moving from left to right along the trend line. The new scaling hence appears to satisfy the desired properties concerning the separation state, while producing a curve that represents the function F_2 , as defined by equation 2.2.

The only point not collapsing onto the curve is the $\varphi = 12^\circ$ ramp of Thomas *et al.* (1994). However, it is difficult to set correctly the onset of separation for this configuration, as the discretisation of the flow deviations is quite large: for example, a change of one degree for the onset of separation would place this point in the set of data. Moreover,

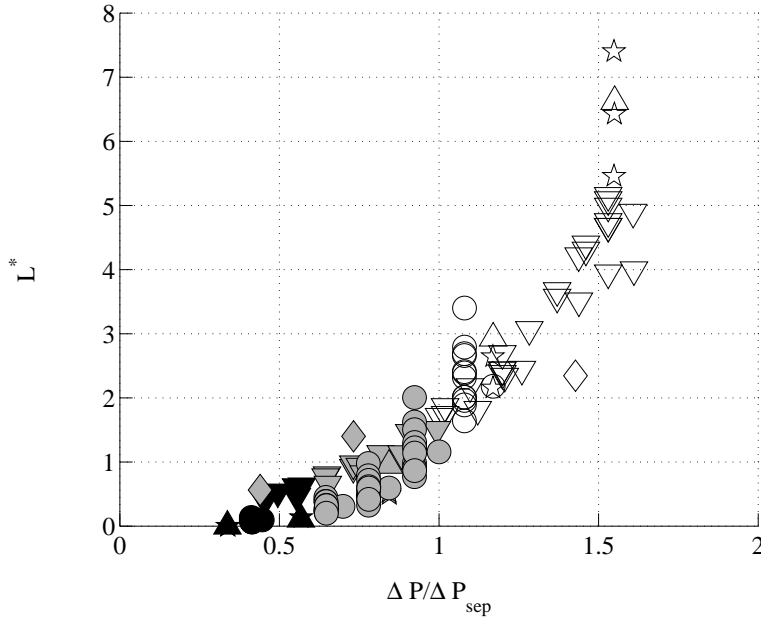


FIGURE 7. New scaling of the interaction length, mass balance based. Symbols according to table 1, colours represent the separation state (black: attached; grey: incipient; white: separated).

TABLE 2. L^* versus the separation states.

Value	Separation state
$L^* \downarrow 0$	Attached flow
$1 < L^* < 2$	Incipient separation
$L^* > 2$	Separated flow

this ramp configuration is on the very limit between two distinct flow solutions (oblique shock and normal shock), and the post shock flow has in either case surpassed the sonic limit (the flow behind the shock is hence completely subsonic), raising questions as to the stability of this particular measurement point. It may be expected that the actual flow organisation for this interaction is particularly sensitive to small variations in the experimental conditions (upstream and downstream of the interaction), resulting possibly in large deviations from the modeled flow organisation.

The effectiveness of the new scaling becomes clear when comparing figure 7 to the scaling from figure 3. Initially, the data points for similar separated states showed a disparity of up to 300%, with an even larger difference for the attached cases. The new scaling makes all points follow the same trend, within a scatter of about the same order as the expected measurement uncertainty, see section 2.1.

2.3. Separation state criteria

In previous section, we used the separation criteria $S^* = \Delta P / \Delta P_{sep}$ to classify the states of separation of the interactions. Unfortunately, as stated in part 2.1, this criteria requires *a priori* knowledge of the onset of separation for a given flow case. This makes it impractical for application since one always needs to have information covering a large range of flow deflection angles to be able to derive the scaling for a single SWBLI flow case. Hence, only experiments which provided this information were included so far, omitting a number of other experimental data sets as well several recent numerical simulations where ΔP_{sep} cannot be determined. To remediate this limitation and to facilitate the application of the scaling to new data points, in this part it is attempted to define an effective separation criteria which is valid for the wide range of Mach numbers and Reynolds numbers under consideration, and which is common to the different interaction geometries. This is done on the basis of the experimental data described in the previous section, subsequently investigating its applicability to the other flow cases where the separation onset is unknown.

Considering first the tendency of the flow to separate, it is noted that flow separation is necessarily initiated close to the wall where $\frac{\partial p}{\partial x} \simeq \frac{\partial \tau}{\partial y}$ (in the viscous sub-layer). This being said, outside the viscous sub-layer one has $\frac{\partial p}{\partial x} \gg \frac{\partial \tau}{\partial y}$. An order of magnitude analysis yields $\frac{\Delta p}{L} \gg \frac{\tau_w}{\delta_0}$, or equivalently $\frac{\Delta p}{\tau_w} \gg \frac{L}{\delta_0}$, a condition that is indeed satisfied by the current experiments, see figure 2. It is therefore justified to consider only the effects of pressure and inertia forces, even though viscous effects exist, remaining however confined to a region very close to the wall. From another point of view, $\tau_w = \rho_w u_\tau^2$, where u_τ is a measure of the velocity defect in the outer part of the turbulent boundary layer. It is known that u_τ decreases for increasing Reynolds numbers, *reducing* the velocity defect while *increasing* $\frac{\Delta p}{\tau_w}$ for given Mach number, flow deviation and stagnation temperature. It should be expected that a smaller velocity defect reduces the tendency of the flow to separate. This is in contradiction with the trend indicated by figure 2, which implies that the flow should be *more separated* for larger $\frac{\Delta p}{\tau_w}$. Considering these two elements, it seems that the wall shear stress is not the correct scaling parameter to describe the tendency of the flow to separate, at least not for the Reynolds number range under consideration, corresponding to fully developed turbulent upstream boundary layers: . laminar or transitional interactions are not considered in the current investigation.

Given the above observations, the occurrence of flow separation is expected to be mostly governed by the inertial forces in the incoming flow, at least at sufficiently high Reynolds numbers. To elaborate this, it is attempted to define a scaling for Δp based on the Euler equations. Hence, the one-dimensional, steady, inviscid momentum balance will be invoked in its differential form to analyse whether the occurrence of separation can be linked to a ratio between the pressure force and the inertia forces in the incoming flow. This with the aim of defining a scaling for Δp for use as separation criterion in equation 2.2. Of course, this simplified approach has several limitations in applying it to the inherently more complicated flow occurring within the interaction. It is done under the hypothesis that it does indeed enable to capture the principal expected driving mechanism for the flow separation state (the balance between pressure and inertia forces) into a simple scaling parameter. Therefore, to evaluate if this simplified approach is indeed in agreement with observations, it will subsequently be verified against the experimental data base.

Under the assumptions stated above, the momentum flux will be related to the pressure gradient as in equation 2.17:

$$-\frac{\partial p}{\partial x} = \frac{\partial(\rho U^2)}{\partial x} \quad (2.17)$$

It is observed that the adverse pressure gradient Δp imposed by the shock system acts approximately over the length of the interaction, decelerating the incoming fluid over the same length. Therefore, the length of interaction L is interpreted as the length scale related to the pressure jump across the interaction. Based on these observations, it is proposed to relate the pressure jump across the interaction to the momentum decrease as follows:

$$-\frac{\Delta p}{L} \sim \frac{\Delta(\rho U^2)}{L} \quad (2.18)$$

Recalling the objective of defining a criterion for flow separation. It is therefore assumed that the flow separates when the incoming streamwise momentum ρU^2 vanishes, in other words, when $\Delta(\rho U^2) = \rho U^2$. Consequently, at separation, the following relation can be written:

$$\Delta p_{sep} \sim \rho_c U_c^2 \quad (2.19)$$

Where U_c and ρ_c are a reference velocity and density respectively for the incoming momentum flux. Given the previous arguments indicating that the flow is governed by pressure and inertia forces in most of the boundary layer, it is expected that ρ_c and U_c are of the order of ρ_e and U_e respectively, where the subscript e is used to refer to the free-stream based value. Inserting the upstream dynamic pressure $q_e = \frac{1}{2}\rho_e U_e^2$, this leads to the following separation criterion:

$$S_e^* = k \frac{\Delta p}{q_e} \quad (2.20)$$

Where k is a constant of order 1 that will be chosen such as to obtain a value of approximately 1 at the onset of separation.

As stated previously, this analysis constitutes a simplification of the actual flow with the specific aim of defining a separation criterion under the hypothesis of capturing the main driving mechanism. To verify whether this approach is justifiable, we will first compare the separation criteria proposed by the equation 2.20 to the original criteria $S^* = \Delta P / \Delta P_{sep}$ used in the previous section for the subset of the data where the onset of separation was documented. The results are plotted versus the Reynolds number figure 8. The results indicate that, despite the large simplifications used to derive the relation 2.20, an efficient estimation of ΔP_{sep} can be derived from the upstream dynamic pressure q_e . First, no remaining influence of the Mach number appears, which means that its influence is accurately taken into account through the dynamic pressure. The ratio is about 3 for the whole set of Reynolds numbers, covering nearly three decades, with a slight decrease over the range of Reynolds numbers from 3 to 2.5, corresponding to 17%. It is remarked that other authors (see Ginoux (1973)) have considered with some success the ratio $\frac{\Delta p}{q_e}$ to scale the shock intensity. They remark that for turbulent boundary layers at sufficient Reynolds numbers, the occurrence of flow separation is Reynolds number independent. The effect of the Reynolds number seems indeed to depend on its magnitude and consequently the flow regime (laminar, transitional, turbulent). In addition, some of the commonly use

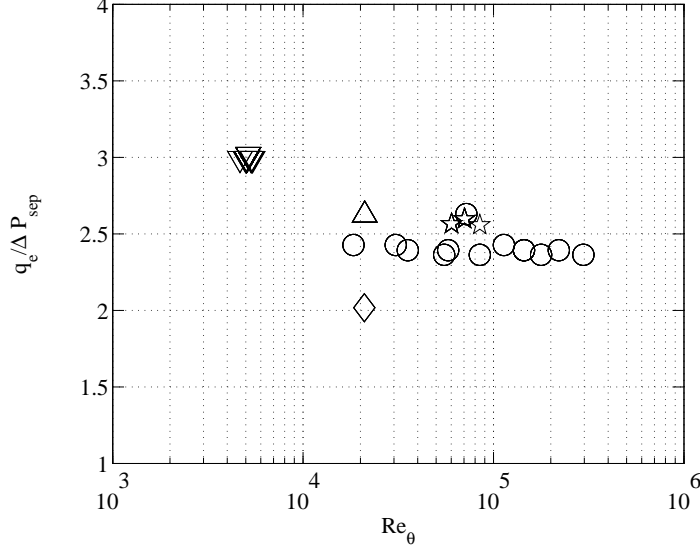


FIGURE 8. Ratio of the dynamic pressure $q_e = \frac{1}{2}\rho_e U_e^2$ and the pressure step needed to separate ΔP_{sep} vs the Reynolds number of the upstream flow. Symbols as in figure 3.

separation criteria (see Summerfield *et al.* (1954); Zukoski (1967); Schmucker (1973)) are a function of the Mach number and the flow deflection only, implying that the occurrence of separation is Reynolds number independent, at least for high Reynolds numbers, in accordance with Ginoux (1973).

Therefore, based on these data we will use the relation 2.20 with k defined as:

$$\begin{aligned} k &= 3.0 \text{ if } Re_\theta \leq 1 \times 10^4 \\ &= 2.5 \text{ if } Re_\theta > 1 \times 10^4 \end{aligned} \quad (2.21)$$

Although this definition of k is based on a limited sub-set of data, including all data from the full compilation shows a good consistency with this behavior, providing further support for the proposed values of k (as will be shown in figure 9). Using the ideal gas law and the definition of the speed of sound, equation 2.20 can be rewritten as:

$$S_e^* = \frac{2k}{\gamma} \frac{\frac{p_{post}}{p_{pre}} - 1}{M_e^2}} \quad (2.22)$$

where $\frac{p_{post}}{p_{pre}}$ is the ratio of the pressure before (p_{pre}) and after (p_{post}) the shock system. For a particular flow organisation (for example compression ramp, incident reflecting shock) and using oblique shock wave theory (see for example Anderson Jr. (1991)), it can be written analytically as a function of the free-stream Mach number M_e , the imposed flow deflection angle φ and the specific heat ratio γ :

$$\frac{p_{post}}{p_{pre}} - 1 = f(M_e, \varphi, \gamma) \quad (2.23)$$

The following final expression is obtained for the separation criterion (assuming a constant specific heat ratio γ):

$$S_e^* = \frac{2k}{\gamma} \frac{f(M_e, \varphi, \gamma)}{M_e^2} = kg_1(M_e, \varphi) \quad (2.24)$$

with k given by the relation 2.21. It is reiterated that g_1 is a function that depends on the particular shock system (for example compression ramp, incident reflecting shock).

In conclusion, it is proposed that, when turbulent flows are considered, the separation criterion can be represented by an analytic relation depending only on the free-stream Mach number, on the flow deflection angle and on the particular shock system. According to the current formulation, the scaling of the shock intensity and the occurrence of separation for turbulent cases are nearly Reynolds number independent, in accordance with the observations from Ginoux (1973). It should therefore be expected that the Reynolds number effects appear mainly through the scaling of the interaction length through the displacement thickness of the upstream flow (see figure 7). It is noted that other effects could also influence the onset of separation, such as for example wall effects (roughness, cooling or heating), as compared to the smooth wall adiabatic cases considered in the present compilation.

The separation criterion S_e^* seems to correctly represent the state of the occurrence of flow separation. This makes it a good candidate for S^* in equation 2.2. As it is only based on external quantities, it can be evaluated for the whole set of available experimental and numerical SWBLI. Results are shown in figure 9. In order to clarify the picture, experiments used in figure 3 are homogeneously represented by a cross symbol, whereas for the new data the symbols given are given according to table 3. In this new compilation, NASA-AMES results have been included, see Thomke & Roshko (1969). These experiments documented the onset of separation for a wide range of Mach numbers ($2 \leq M \leq 5$) at high Reynolds numbers. They have however been omitted from the previous compilation (see figure 7). The reason for this is that the criteria to qualify the separation state in these experiments was biased towards too high angles of deviations (the measurement methods employed in their study are relatively insensitive to small regions of separation), as has been reported by Settles *et al.* (1976). As this bias is confirmed by our current compilation, we have not considered them previously in the evaluation of ΔP_{sep} and their state of separation is not reported on the figures. Nevertheless, as shown figure 9, they follow well the general trend whatever the separation state or the Mach number considered, confirming that the data is coherent with the proposed scaling. Similarly, the state of separation of the heated wall experiments from IUSTI were not documented. They are reported on the figure, with the state of separation of the adiabatic interaction considered at the same flow deviation. Despite the uncertainty of the effect of wall heating on the separation state, and of the applicability of the approximation given by the relations 2.20 and 2.21 for non-adiabatic wall conditions (which could not be verified so far), this set of experiments follows the same general trend.

A best fit of a power law (see the equation in the figure legend) is reported on the figure 9. It corresponds to a R square value of 0.9428. A good collapse of the whole set of data is obtained. Only the data from Polivanov *et al.* (2009) differ from the compilation. Despite no significant effects has been found in these experiments on the dimensionless frequency (or Strouhal number) for the unsteady properties, it can be remarked from their Schlieren visualisations that the reflected shock is relatively thick: this can be interpreted as significative three dimensional effects as well as important shock dynamics. It is not known whether the mean shock trace or the most upstream shock position has been used to determine the interaction length. The latter case would be in accordance with the

TABLE 3. Interactions considered in figure 9.

Short	Institute	Literature
<i>Incident shock reflections</i>		
IUSTI	IUSTI, Marseille	Laurent (1996)
ITAM	ITAM, Novosibirsk	Polivanov <i>et al.</i> (2009)
TUD	Delft University of Technology	Souverein <i>et al.</i> (2009), Humble (2009), Humble <i>et al.</i> (2009b), Souverein <i>et al.</i> (2010), Souverein (2010)
<i>Compression ramps</i>		
IUSTI	IUSTI, Marseille	Debiève (1983)
UP	University of Princeton	Ringuette <i>et al.</i> (2009)(experiment), Wu & Martin (2008) (DNS)
UA	University of Texas at Austin	Erengil & Dolling (1991a), Erengil & Dolling (1991b), Hou (2003), Ganapathisubramani <i>et al.</i> (2007b)
NA	NASA Ames Research Center	Thomke & Roshko (1969)
US	University of Southampton	Touber & Sandham (2009a) (LES)
<i>Incident shock reflections:</i>		
△	IUSTI: $Re_\theta = 5 \times 10^3$, $M_e = 2.3$, $T_p/T_f = 2.0$	
○	ITAM: $Re_\theta = 2.8 \times 10^3$, $M_e = 2.0$	
★	TUD: $Re_\theta = 50 \times 10^3$, $M_e = 1.7$ and 2.1	
□	US: $Re_\theta = 5 \times 10^3$, $M_e = 2.3$	
<i>Compressions ramps:</i>		
▽	IUSTI: $Re_\theta = 5 \times 10^3$, $M_e = 2.3$	
◇	UP: $Re_\theta = 2.3 \times 10^3$, $M_e = 2.9$, experiment and DNS	
▷	UA: $Re_\theta = 26 \times 10^3$, $M_e = 5.0$	
◁	UA: $Re_\theta = 35 \times 10^3$, $M_e = 2.0$	
*	NA: $Re_\theta = 18 - 300 \times 10^3$, $2 \leq M_e \leq 5$	

approximate magnitude of the overestimation. In addition, this interaction appears to be of the transitional type ($Re_x \approx 2 - 3 \times 10^6$). This regime likely requires a specific Reynolds number dependent scaling for ΔP_{sep} . The other data follow the same trend as data used in figure 7, notwithstanding the fact that the data set now covers the full range from large Reynolds number experimental data (for example the TUD, UA, or NA experiments) down to low Reynolds number numerical results (respectively the US Mach 2.3 reflection interaction case and the UP Mach 3 compression corner case). Using the new scaling, all points follow the best fit curve to within a disparity that is at least an order of magnitude smaller than the initial one (see figure 2) and about the same order as the expected measurement uncertainty, see section 2.1. As a remark, it is noted that apart from measurement uncertainties, part of the scatter on the rescaled data will certainly also have physical causes, i.e. effects that are not taken into account by the model (for instance effects induced by differences in the experimental setups, the flow facilities, etc.).

Given the scaling proposed in figure 9, at least two options for controlling the interaction can be suggested. To suppress flow separation, the trend line indicates that one should either act on S_e^* , imposing $\Delta p \rightarrow 0$, or on $\frac{L}{\delta_{in}^*}$, imposing $\delta_{in}^* \rightarrow 0$. The first option ($\Delta p \rightarrow 0$) actually modifies the physical separation state of the flow. In the case of the second option, keeping the value of S_e^* fixed (in other words, $\varphi = cst$ and $M_e = cst$) means that the separation state is inherently prescribed, while $\frac{L}{\delta_{in}^*}$ is a constant deter-

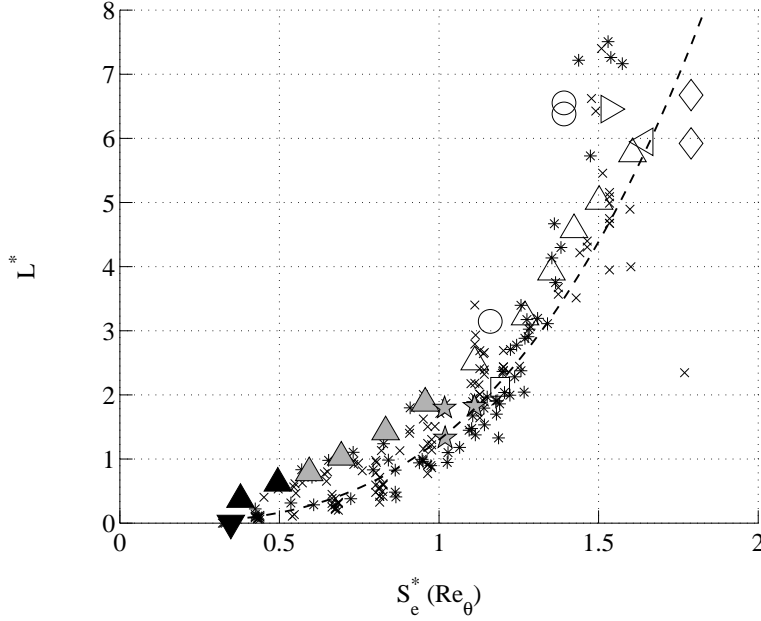


FIGURE 9. New scaling of the interaction length, mass balance based. Colours represent the separation state (black: attached; grey: incipient; white: separated). \times : experiments used in figure 3 other symbols given by table 3. Dashed line: best fit line ($a * x^b$, with $a = 1.3$ and $b = 3$).

mined by the trend line. The second option hence implies that to reattach the flow, one should make L vanish, which is achieved when $\delta_{in}^* \rightarrow 0$, in other words when $Re_{\delta^*} \rightarrow 0$. For upstream control, this appear to be the only option when the interaction geometry and free-stream conditions are fixed. It is reiterated that this approach does not alter the flow separation state, but that it diminishes the separation bubble size by a reduction in the interaction size. Of course, these observation are subject to the assumptions used in the derivation of the scaling. For example, things might look differently locally if the flow becomes subject to significant spanwise modulations (3D-effects). Nevertheless, in a global (spanwise averaged) sense they might however retain a certain validity also in these cases.

Finally, some comments can be derived concerning the three dimensional effects in the SWTBLI experiments. It is well known that wind tunnel experiments can develop significant three dimensional organisation in such flows, due to the lateral interactions developing on the side walls. In cases of separated interactions, large spanwise structures can develop in the separated region, despite the mean head shock remains qualitatively two dimensional. (see Dupont *et al.* (2005); Garnier (2009)). In general, the reflection geometry is considered as more sensitive to such lateral effects than the compression corner configurations. Nevertheless, the figure 9 does not highlight any discrepancies between these two families of SWTBLI, even for massive separated interactions, except perhaps for the Polivanov data (see previous comments). Therefore, it is suggested that if the the present results can be influenced by three dimensional effects, in a global (spanwise averaged) sense they might however retain a certain validity

3. Discussion

3.1. Mach Reynolds dependencies

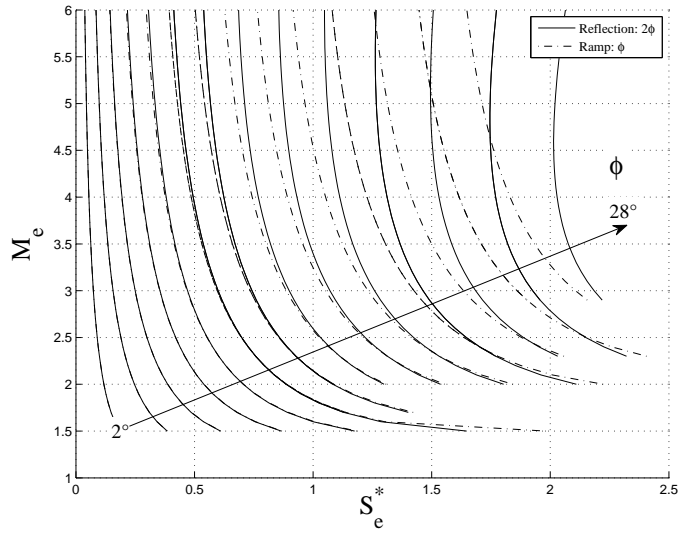
The separation state criteria S_e^* depends only slightly on the Reynolds number of the upstream boundary layer through the coefficient k (see relations 2.21 and 2.24), a dependence that seems to vanish in the limit of large Reynolds numbers ($Re_\theta > 10^4$). On the contrary, there is a direct dependence on the Mach number and the imposed flow deflection angle (see eq. 2.24). It enables the graphical determination of the Mach-deflection angle combination leading to a particular tendency of the flow to separate. An average value of k of 2.8 has been used in this case. As can be observed from figure 10(b), for small Mach numbers, the incident shock deflection angle can be multiplied by two to obtain the equivalent ramp angle that yields the same value of S_e^* . From the figure it can be read that, for example, the same flow separation state should be expected for the Mach=5, $\varphi = 28^\circ$ compression ramp as for the Mach=3, $\varphi = 24^\circ$ ramp.

It is observed that due to the Mach number effect, the flow over a $\varphi = 20^\circ$ ramp at Mach=2 should be more separated than a ramp at Mach=3 for the same deflection angle. This is clearly illustrated by figure 10(a), confirming the well known property that an increase in Mach number tends to postpone the onset of flow separation at constant deflection angle (see also Ginoux (1973)). It is noted that the current results equally indicate that an increase in M_e leads to a reduction of the interaction length at constant φ (S_e^* decreases and $G_3(M_e, \varphi)$ increases; figure 9 and equation 2.15 now show that L^* must decrease and consequently also L for constant δ_{in}^*). In addition, it is remarked that for a Mach=3 interaction, the flow will always be separated for ramp angles larger than $\varphi = 16 - 18^\circ$ (incident shock deflections of $\varphi = 8 - 9^\circ$). Alternatively, a ramp of approximately $\varphi = 6^\circ$ (an incident shock deflection of $\varphi = 3^\circ$) will be attached for any Mach number that does not involve a normal shock solution.

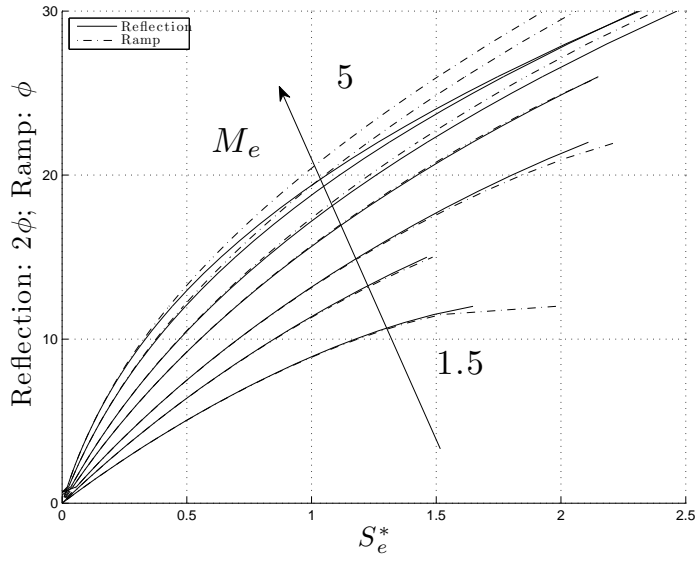
3.2. A new spatial scaling for turbulent fields in SWBLI

The common choice for the longitudinal length scale is the interaction length L . For the scaling of the wall normal length scale, one might intuitively choose a characteristic length related to the upstream boundary layer (for example δ_0 or δ^*). However, such quantities can by definition not take into account the variations in interaction properties due to different imposed flow deflection angles. The question of the scaling of the wall normal length scale will be addressed in the following, using data obtained in two supersonic facilities, respectively the TST-27 wind tunnel at the Delft University of Technology and the S8 wind tunnel at the Institut Universitaire des Systèmes Thermiques Industriels (IUSTI) to verify the results.

The most important parameter discriminating both facilities is the momentum thickness based Reynolds number, which is a factor 10 higher for the TST-27 as compared to the S8. The current investigation has taken advantage of the combined use of both facilities to obtain measurements of the same flow phenomenon over a range of measurement conditions (Reynolds number, Mach number, shock strength, interaction control), using different measurement systems, enabling a thorough comparison and validation of the observations. The flow cases under consideration have already been extensively documented (Dupont *et al.* (2005); Dussauge *et al.* (2006); Dupont *et al.* (2006, 2008); Souverein *et al.* (2009, 2010); Souverein & Debiève (2010)). The incoming boundary layers are turbulent and fully developed. The main aerodynamic parameters are listed in table 4, where the boundary layer thickness δ_0 was based on 99% of the external velocity U_e , δ^* is the displacement thickness, θ is the momentum thickness and H the shape factor.



(a)



(b)

FIGURE 10. Dependence of S_e^* on the Mach number and the flow deflection: (a) Mach dependence M_e (ϕ -discretisation [2:2:28]deg); (b) Flow deflection dependence ϕ [deg] (M_e -discretisation [1.5 1.75 2.0 2.5 3 4 5]). Figures include the theoretical dependence of S_e^* on M_e and ϕ for both the incident reflection and the compression ramp.

The full field quantitative velocity data used in this investigation, including the mean and turbulent velocity fields, were obtained by means of PIV. The data acquisition and post processing were done using the systems and software that were available in each respective laboratory:

TABLE 4. Measurement conditions

	M_e	φ	$\delta_0[mm]$	$\delta^*[mm]$	$\theta[mm]$	H	Re_θ
TST-27	1.69	6.0	17.2	3.3	1.4	2.4	50,000
S8	2.28	5.5; 8.0; 9.5	10.2	3.0	0.9	3.5	5,000

• At the TU Delft, a *La Vision Davis 7.2* acquisition system was used with a PTU 9 timing unit. Data processing was done with in house developed WIDIM software employing an iterative multi-grid deforming window correlation scheme (see Scarano & Riethmuller (1999)).

• At the IUSTI, a *Dantec Dynamics* system was used for the data acquisition, timing, and data processing

In both cases, a dimensionless spatial resolution of $y/\delta \approx 2 - 2.9 \times 10^{-2}$ has been used to define the PIV interrogation window size. The seeding systems were also different: Di*2-ethylhexyl sebacate (DEHS) droplets at TU-Delft, whereas incense smoke was used at IUSTI. See previous references for detailed description of the experiments. In both facilities, the inflow conditions comprise a canonical zero pressure gradient supersonic ($M < 5$) turbulent boundary layer.

As detailed in table 4, four cases have been considered:

• two incipient cases in both facilities, with Mach numbers of $M_e = 1.7$ and 2.3 respectively

• two low Reynolds numbers separated interactions for $M_e = 2.3$

The incipient cases have been adjusted to present similar probability of reverse flow, with a 50% probability near the wall (see Souverein *et al.* (2010)).

The turbulent velocity fields obtained within the interaction regions were shown in Souverein *et al.* (2010). In all four cases, the turbulent fields exhibit a resemblance: a highly turbulent region develops downstream of the foot of the reflected shock, related to the formation of large coherent scales in the mixing layer which develops downstream of this point (Dupont *et al.* (2006, 2008); Souverein *et al.* (2009)). Nevertheless, the extent of the development of this region was found to depend on the state of the interactions (incipient or separated), see figure 6 in Souverein *et al.* (2010).

The question of the physically correct scaling of the wall normal length scale will now be re-addressed. This will be done using the scaling analysis of the section 2.2. Indeed, it has been shown that only one length scale (δ^* or other) cannot suffice to describe the spatial extent of the interaction. Therefore, the non-dimensional length scale L^* defined by equation 2.15 will be introduced. Using this equation one can scale the wall normal coordinate by L as follows:

$$Y^* = \frac{y}{LG_3(M_e, \varphi)} = \frac{y}{\delta_{in}^* L^*} \quad (3.1)$$

where $G_3(M_e, \varphi)$ is an analytical function, see equation 2.16.

Figure 11 shows the result obtained when scaling the wall normal coordinate using equation 3.1. The extent of the vertical axis is the same for the four cases. The unity value for the y -axis, indicated by the black dashed line, corresponds to the approximate extent of the highly turbulent region developing downstream of the head shock. In all

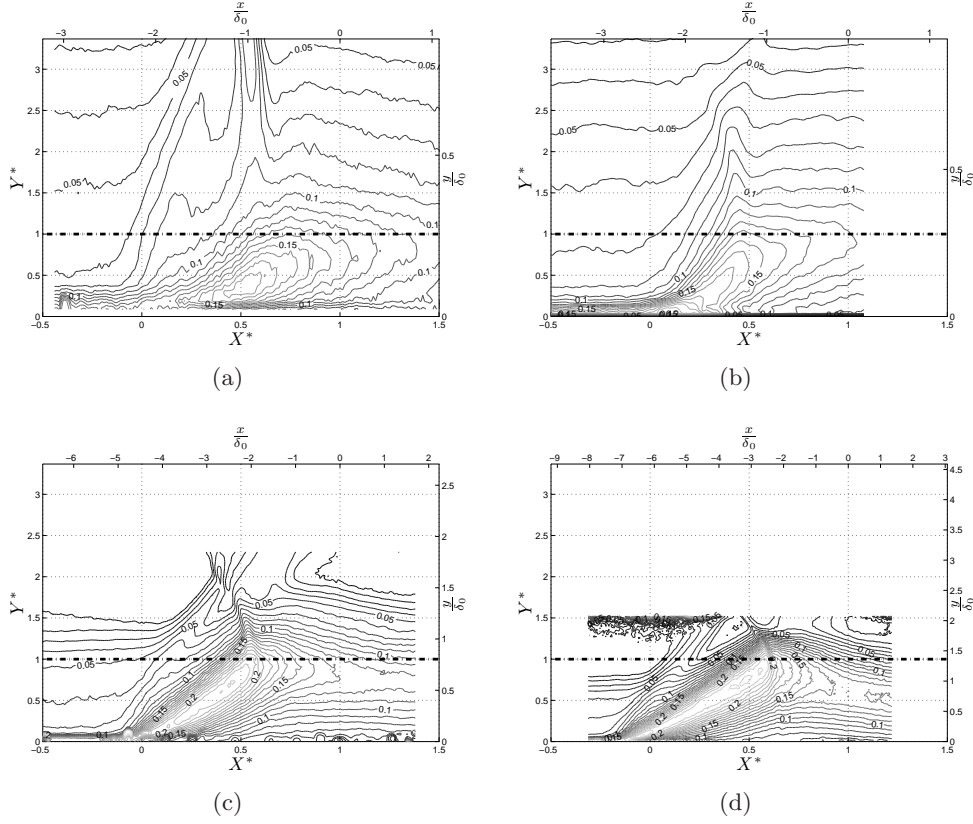


FIGURE 11. U -component fluctuations (RMS) normalized by the free-stream velocity using the L^* scaling option: (a) high Reynolds number incident, 6.0° ; (b) low Reynolds number incident, 5.5° ; low Reynolds number separated cases, (c) 8.0° and (d) 9.5° . Fluctuation values are normalised by the free-stream velocity. The black horizontal dashed line indicates the unit-value for the y -axis. The horizontal and vertical scale on the top and right axis represent the coordinates normalised by δ_0 for reference.

cases, the interactions are included in a 1×1 box, which shows that the scaling defined by equation 2.15 is relevant to compare turbulent fields of different interactions.

4. Conclusions

A scaling analysis was made, aimed at reconciling the observed discrepancies between interactions documented in literature (geometry, Reynolds number effects, Mach number effects, shock intensity, ...). As part of this analysis, a separation criterion has been formulated that depends on the free-stream Mach number and the flow deflection angle only. It successfully classifies the separation states for a large scope of documented interactions (compression ramp and incident reflecting shock) over a large Reynolds number and Mach number range:

$$S_e^* = k \frac{\Delta p}{q_e} = k g_1(M_e, \varphi) \quad (4.1)$$

$$S_e^* < 1 \quad \text{Attached flow}$$

$$S_e^* \geq 1 \quad \text{Separated flow}$$

where k is a constant which depends slightly on the Reynolds number, see eq. 2.21. In addition, a scaling approach has been derived for the interaction length based on the mass balance:

$$L^* = \frac{L}{\delta_{in}^*} G_3(M_e, \varphi) \quad (4.2)$$

$$\text{with: } G_3(M_e, \varphi) = \frac{\sin(\beta) \sin(\varphi)}{\sin(\beta - \varphi)}$$

The separation criterion S_e^* in combination with the normalised L^* represents a single trend line onto which all data for a large scope of documented interactions over a large Reynolds and Mach range fall together with a moderate scatter of approximately $\pm 15\%$, which is of the same order as the measurement uncertainty. This curve is valid both for compression ramp interactions and for incident reflecting shock interactions. A similar formulation has been obtained from the momentum balance. Both results are equivalent.

A scaling for the wall normal coordinate has been defined based on this scaling approach for the interaction length: $Y^* = \frac{y}{L G_3(M_e, \varphi)}$. It produces a large resemblance in the geometric organisation of the turbulent flow fields within the interactions for the considered flow cases, independent of the Mach number and Reynolds number and of the separation state.

Concerning the Reynolds number and Mach number effects, it can be concluded that for turbulent boundary layers, the onset of flow separation is nearly Reynolds number independent. It seems to be governed principally by the Mach number and the imposed flow deflection angle; an increase in Mach number tends to reduce the deflection angle for the onset of flow separation. The Reynolds number effects appear implicitly through the scaling of the interaction length by the displacement thickness of the incoming boundary layer. However, the interaction length is also governed by the Mach number through a correction factor that also involved the imposed flow deflection angle.

Acknowledgments

This research was a joint effort of between TU Delft and IUSTI and it was performed during the research period of the lead author at these institutes. Part of this work was carried out with support from the Research Pole CNES/ONERA *Aérodynamique des Tuyères et Arrière-Corps* (ATAC) and a grant of the European STREP UFAST (contract n°AST4-CT-2005-012226). Their support is gratefully acknowledged.

Appendix

In analogy to the mass conservation approach in section 2.2, the same analysis has been applied for the momentum conservation. This is done for both the incident shock reflection and the compression ramp case. In the end, a common formulation is derived. For completion, it is noted that the length scale for the momentum deficit is obtained by integrating the momentum flux within the boundary layer profile (with H the shape factor) as follows:

$$\begin{aligned} \frac{1}{\rho_e U_e^2} \int_0^\infty (\rho_e U_e^2 - \rho U^2) dy &= \int_0^\infty \frac{\rho U}{\rho_e U_e} \left(1 - \frac{U}{U_e}\right) dy \\ &+ \int_0^\infty \left(1 - \frac{\rho U}{\rho_e U_e}\right) dy \\ &= \theta + \delta^* = \theta(1 + H) \end{aligned} \quad (4.1)$$

Incident shock reflection

First, the incident shock reflection case is analysed. Evaluating the X -momentum equation over the control volume shown in figure 5(a) the following equality is obtained for the inviscid flow case:

$$\rho_1 U_1^2 H_{cv} + \rho_2 U_2 V_2 L_{cv} - \rho_3 U_3^2 H_{cv} = (p_3 - p_1) H_{cv} \quad (4.2)$$

At the same time, the following equality is obtained for the case with interaction:

$$\begin{aligned} \rho_1 U_1^2 (H_{cv} - \theta_1(1 + H_1)) + \\ \rho_2 U_2 V_2 (L_{cv} - L) - \\ \rho_3 U_3^2 (H_{cv} - \theta_3(1 + H_3)) = (p_3 - p_1) H_{cv} \end{aligned} \quad (4.3)$$

Eliminating the pressure term, the following equation is obtained for the interaction length for the shock reflection case:

$$L = \frac{\rho_3 U_3^2 \theta_3 (1 + H_3) - \rho_1 U_1^2 \theta_1 (1 + H_1)}{\rho_2 U_2 V_2} \quad (4.4)$$

In analogy to the result from the mass conservation approach, the interaction length obtained from the momentum conservation approach is completely determined by the upstream and downstream boundary layer momentum thickness and shape factor, the densities and velocities being specified by oblique shock wave theory. The equation is independent of the height and length of the control volume as long as the interaction is included.

Compression ramp

Next, the compression ramp case is analysed. Evaluating the X -momentum equation over the control volume shown in figure 5(b) the following equality is obtained for the inviscid flow case:

$$\rho_1 U_1^2 H_{cv_1} - \rho_2 U_2^2 H_{cv_2} \cos(\varphi) = (p_2 - p_1) H_{cv_1} \quad (4.5)$$

At the same time, the following equality is obtained for the case with interaction:

$$\begin{aligned} & \rho_1 U_1^2 (H_{cv} - \theta_1(1 + H_1)) - \\ & \rho_2 U_2^2 L \sin(\varphi) \cos(\varphi) - \\ & \rho_2 U_2^2 (H_{cv_2} - \theta_2(1 + H_2)) \cos(\varphi) = (p_2 - p_1) H_{cv_1} \end{aligned} \quad (4.6)$$

Eliminating the pressure term, the following equation is obtained for the interaction length for the compression ramp case:

$$L = \frac{\rho_2 U_2^2 \theta_2 (1 + H_2) \cos(\varphi) - \rho_1 U_1^2 \theta_1 (1 + H_1)}{\rho_2 U_2^2 \sin(\varphi) \cos(\varphi)} \quad (4.7)$$

Again, the interaction length obtained from the momentum conservation approach is completely determined by the upstream and downstream boundary layer momentum thickness and shape factor, the densities and velocities being specified by oblique shock wave theory. The equation is independent of the height and length of the control volume as long as the interaction is included.

Common formulation

In analogy to the mass conservation approach, it is attempted to find a common formulation for equations 4.4 and 4.7. To this aim, the denominator of each equation is reformulated in terms of the upstream conditions by means of the oblique shock wave relations. Using the fact that the velocity tangent to the shock is conserved, the following equality is obtained:

$$U_1 \cos(\beta) = U_2 \frac{\cos(\beta - \varphi)}{\cos(\varphi)} \quad (4.8)$$

Similarly, considering mass conservation across the shock for the compression ramp case gives:

$$U_1 \cos(\beta) = U_2 \cos(\beta - \varphi) \quad (4.9)$$

Using equations 2.10 and 2.11, rewriting each of the equalities above and substituting all in their respective relations (equation 4.4 for the incident shock interaction and 4.7 for the compression corner) gives an equation of the same form, which can be written as follows when using the subscripts *in* and *out* for the inflow and outflow conditions respectively and when defining the momentum deficit as $I^* = \rho U^2 \theta (1 + H)$:

$$\frac{L}{\theta_{in}(1 + H_{in})} = g_3(M_e, \varphi) g_4(M_e, \varphi) \left(\frac{I_{out}^* C(\varphi)}{I_{in}^*} - 1 \right) \quad (4.10)$$

Where:

$$\text{Shock reflection: } C(\varphi) = 1$$

$$\text{Compression ramp: } C(\varphi) = \cos(\varphi)$$

And with $g_3(M_e, \varphi)$ a ratio of sine functions, and $g_4(M_e, \varphi)$ a ratio of cosine functions:

$$g_3(M_e, \varphi) = \frac{\sin(\beta - \varphi)}{\sin(\beta) \sin(\varphi)}; \quad g_4(M_e, \varphi) = \frac{\cos(\beta - \varphi)}{\cos(\beta) \cos(\varphi)} \quad (4.11)$$

The factor $C(\varphi)$ appears in the compression ramp equation due to the definition of U_{out} : the X -momentum is considered, while the outgoing velocity is aligned with the ramp. The equation gives an alternative algebraic relation for the interaction length as

a function of M_e , φ , the incoming boundary layer fullness, and the momentum deficit ratio between the incoming boundary layer and the outgoing boundary layer. In analogy to the mass conservation result, it can be concluded that the interaction length is also a direct consequence of the momentum deficit ratio between the incoming and outgoing boundary layer. The proper scaling for the vertical axis in terms of the momentum deficit ratio, with \hat{L} the non-dimensional interaction length and with $C(\varphi)$ defined by equation 4.10, would hence be:

$$\hat{L} = \frac{L}{\theta_{in}(1 + H_{in})} G_3(M_e, \varphi) G_4(M_e, \varphi) = \frac{I_{out}^*}{I_{in}^*} C(\varphi) - 1 \quad (4.12)$$

With:

$$G_3(M_e, \varphi) = g_3(M_e, \varphi)^{-1} = \frac{\sin(\beta) \sin(\varphi)}{\sin(\beta - \varphi)}$$

$$G_4(M_e, \varphi) = g_4(M_e, \varphi)^{-1} = \frac{\cos(\beta) \cos(\varphi)}{\cos(\beta - \varphi)}$$

REFERENCES

- ANDERSON JR., J. D. 1991 *Fundamentals of Aerodynamics*, 2nd edn. McGraw-Hill, New-York.
- ARDONCEAU, P. L. 1984 The structure of turbulence in a supersonic shock-wave/boundary-layer interaction. *AIAA Journal* **22** (9), 1254–1262.
- ATKIN, C. J. & SQUIRE, L. C. 1992 A study of the interaction of a normal shock wave with a turbulent boundary layer at Mach numbers between 1.30 and 1.55. *European J. Mechanics* **11** (1), 93–118.
- BENKEMOUN, L. & SALAUN, M. 1988 Développement d'une couche limite turbulente supersonique sur une paroi chauffée: Propriétés du champ turbulent et exploitation théorique. *Tech. Rep.*
- BERESH, S. J., CLEMENS, N. T. & S.DOLLING, D. 2002 Relationship between upstream turbulent boundary layer velocity fluctuations and separation shock unsteadiness. *AIAA Journal* **40** (12), 2412–2422.
- BOURGOING, A. & REIJASSE, P. H. 2005 Experimental analysis of unsteady separated flows in a supersonic planar nozzle. *Shock Waves* **14** (4), 251–258.
- BRUCE, P. J. K. & BABINSKY, H. 2008 Unsteady shock wave dynamics. *Journal of Fluid Mechanics* **603**, 463–473.
- BRUSNIAK, L. & DOLLING, D. S. 1994 Physics of unsteady blunt-fin-induced shock wave/turbulent boundary layer interactions. *Journal of Fluid Mechanics* **273**, 375–409.
- BUENO, P. C. 2006 The effects of upstream mass injection by vortex generator jets on shock-induced turbulent boundary layer separation. Doctoral thesis, The University of Texas at Austin.
- BUR, R., BENAY, R., GALLI, A. & BERTHOUBE, P. 2008 Experimental and numerical study of forced shock-wave oscillations in a transonic channel. *Aerospace Science and Technology* **10**, 265–278.
- CHAPMAN, D. R., KUEHN, D. M. & LARSON, H. K. 1957 Investigation of separated flow in supersonic and subsonic streams with emphasis of the effect of transition. *Tech. Rep.*
- CHERRY, N. J., HILLIER, R. & LATOUR, M. E. M. 1984 Unsteady measurements in a separated and reattaching flow. *Journal of Fluid Mechanics* **144**, 13–46.
- CLEMENS, N. T. & NARAYANASWAMY, V. 2009 Shock/turbulent boundary layer interactions: Review of recent work on sources of unsteadiness. In *39th Fluid Dynamics Conference and Exhibit, San Antonio, Texas, USA, AIAA-2009-3710*.
- DEBIÈVE, J. F. 1983 Etude d'une interaction turbulence- onde de choc. Thèse d'état, Université d'Aix-Marseille.
- DÉLÉRY, J. M. & DUSSAUGE, J. P. 2009 Some physical aspects of shock wave/boundary layer interactions. *Shock Waves* **19** (6), 453–468.
- DÉLÉRY, J. M. & MARVIN, J. G. 1986 Shock wave - boundary layer interactions. *Tech. Rep.*
- DOLLING, D. S. 2001 Fifty years of shock-wave/boundary-layer interaction research: what next. *AIAA Journal* **39** (8), 1517–1531.
- DOLLING, D. S. & BRUSNIAK, L. 1989 Separation shock motion in fin, cylinder, and compression ramp-induced turbulent interactions. *AIAA Journal* **27** (6), 734–742.
- DOLLING, D. S. & MURPHY, M. T. 1983 Unsteadiness of the separation shock wave structure in a supersonic compression ramp flowfield. *AIAA Journal* **21** (12), 1628–1634.
- DOLLING, D. S. & OR, C. T. 1985 Unsteadiness of the shock wave structure in attached and separated compression ramp flows. *Experiments in Fluids* **3**, 24–32.
- DUPONT, P., HADDAD, C., ARDISSONE, J. P. & DEBIÈVE, J. F. 2005 Space and time organisation of a shock wave/turbulent boundary layer interaction. *Aerospace Science and Technology* **9** (7), 561–572.
- DUPONT, P., HADDAD, C. & DEBIÈVE, J. F. 2006 Space and time organization in a shock induced boundary layer. *Journal of Fluid Mechanics* **559**, 255–277.
- DUPONT, P., PIPONNIAU, S., SIDORENKO, A. & DEBIÈVE, J. F. 2008 Investigation of an oblique shock reflection with separation by PIV measurements. *AIAA Journal* **46** (6), 1365–1370.
- DUSSAUGE, J. P., DUPONT, P. & DEBIÈVE, J. F. 2006 Unsteadiness in shock wave boundary layer interactions with separation. *Aerospace Science and Technology* **10**, 85–91.
- ERENGLI, M. E. & DOLLING, D. S. 1991a Correlation of separation shock motion with pressure fluctuations in the incoming boundary layer. *AIAA Journal* **29** (11), 1868–1877.

- ERENGIL, M. E. & DOLLING, D. S. 1991*b* Unsteady wave structure near separation in a Mach 5 compression ramp interaction. *AIAA Journal* **29** (5), 728–735.
- FREY, M. & HAGEMANN, G. 1998 Status of flow separation prediction in rocket nozzles. *AIAA Paper* (98-3619).
- FREY, M. & HAGEMANN, G. 2000 Restricted shock separation in rocket nozzles. *Journal of Propulsion and Power* **16** (3), 478–484.
- GANAPATHISUBRAMANI, B., CLEMENS, N. T. & DOLLING, D. S. 2007*a* Effects of upstream boundary layer on the unsteadiness of shock-induced separation. *Journal of Fluid Mechanics* **585**, 369–394.
- GANAPATHISUBRAMANI, B., CLEMENS, N. T. & DOLLING, D. S. 2007*b* Effects of upstream coherent structures on low-frequency motion of shock-induced turbulent separation. In *45th AIAA Aerospace Sciences Meeting and Exhibit, Reno, Nevada*.
- GARNIER, E. 2009 Stimulated detached eddy simulation of three-dimensional shock / boundary layer interaction. *Shock Waves* **19** (6), 479–486.
- GINOUX, J. J. 1973 Interaction entre ondes de choc et couches limites. In *Chocs et ondes de choc, Tome II* (ed. A. L. Jaumotte). Masson & Cie.
- GREEN, J.E. 1970 Reflexion of an oblique shock wave by a turbulent boundary layer. *Journal of Fluid Mechanics* **40**, 81–95.
- HOU, YONGXI X. 2003 Particle image velocimetry study of shock-induced turbulent boundary layer separation. Doctoral thesis, The University of Texas at Austin.
- HUMBLE, R. A. 2009 Unsteady flow organization of a shock wave/boundary layer interaction. Doctoral thesis, Delft University of Technology.
- HUMBLE, R. A., ELSINGA, G. E., SCARANO, F. & VAN OUDHEUSDEN, B. W. 2009*a* Three-dimensional instantaneous structure of a shock wave/turbulent boundary layer interaction. *Journal of Fluid Mechanics* **622**, 33–62.
- HUMBLE, R. A., SCARANO, F. & VAN OUDHEUSDEN, B. W. 2009*b* Unsteady aspects of an incident shock wave/turbulent boundary layer interaction. *Journal of Fluid Mechanics* **635**, 47–74.
- KIYA, M. & SASAKI, K. 1983 Structure of a turbulent separation bubble. *Journal of Fluid Mechanics* **137**, 83–113.
- KUNTZ, D. W., AMATUCCI, V. A. & ADDY, A. L. 1987 Turbulent boundary-layer properties downstream of the shock-wave / boundary-layer interaction. *AIAA Journal* **25** (5), 668–675.
- LAURENT, H. 1996 Turbulence d'une interaction onde de choc- couche limite sur paroi plane adiabatique ou chauffée. Thèse de 3ème cycle, Université d'Aix-Marseille II.
- PIPONNAU, S. 2009 Instationnarités dans les décollements compressibles: cas des couches limites soumises à ondes de choc. Thèse de doctorat, Université de Provence.
- PIPONNAU, S., DUSSAUGE, J. P., DEBIÈVE, J. F. & DUPONT, P. 2009 A simple model for low-frequency unsteadiness in shock-induced separation. *Journal of Fluid Mechanics* **629**, 87–108.
- PIROZZOLI, S., BEER, A., BERNARDINI, M. & GRASSO, F. 2009 Computational analysis of impinging shock-wave boundary layer interaction under conditions of incipient separation. *Shock Waves* **19** (6), 487–497.
- PIROZZOLI, S. & GRASSO, F. 2006 Direct numerical simulation of impinging shock wave / turbulent boundary layer interaction at $M=2.25$. *Physics of Fluids* **18**, 065113–17.
- PLOTKIN, K.J. 1975 Shock wave oscillation driven by turbulent boundary layer fluctuations. *AIAA Journal* **13** (8), 1036–1040.
- POLIVANOV, P., SIDORENKO, A. & MASLOV, A. 2009 Report on the measurement of shock reflection by Mach=2.0: Final report. UFAST Deliverable 3.3.6. Institute of Theoretical and Applied Mechanics.
- RINGUETTE, M.J., WU, M. & MARTIN, M. P. 2008 Low Reynolds number effects in a Mach 3 shock/turbulent-boundary-layer interaction. *AIAA Journal* **46** (7), 1884–1887.
- RINGUETTE, M. J., BOOKEY, P., WYCKHAM, C. & SMITS, A. J. 2009 Experimental study of a Mach 3 compression ramp interaction at $Re_\theta = 2400$. *AIAA Journal* **47** (2), 373–385.
- SCARANO, F. & RIETHMULLER, M. L. 1999 Iterative multigrid approach in PIV image processing with discrete window offset. *Experiments in Fluids* **26**, 513–523.
- SCHMUCKER, R. 1973 Strömungsvorgänge beim Betrieb überexpandierter Düsen chemischer

- Raketentriebwerke (Flow Processes in Overexpanded Nozzles of Chemical Rocket Engines). *Tech. Rep.*. Technical University Munich.
- SELIG, M. S., ANDREOPOULOS, J., MUCK, K. C., DUSSAUGE, J. P. & SMITS, A. J. 1989 Details of a shock - separated turbulent boundary layer at a compression corner. *AIAA Journal* **27** (7), 862–869.
- SETTLES, G. S., BOGDONOFF, S. M. & VAS, I. E. 1976 Incipient separation of a supersonic turbulent boundary layer at high Reynolds number. *AIAA Journal* **14** (1), 50–56.
- SETTLES, G. S., FITZPATRICK, T. J. & BOGDONOFF, S. M. 1979 Detailed study of attached and separated compression corner flowfields in high Reynolds number supersonic flow. *AIAA Journal* **17**, 579–585.
- SMITS, A. J. & DUSSAUGE, J. P. 2006 *Turbulent shear layers in supersonic flow*, 2nd edn. AIP Press.
- SMITS, A. J. & MUCK, K. C. 1987 Experimental study of three shock wave / turbulent boundary layer interactions. *Journal of Fluid Mechanics* **182**, 291–314.
- SOUVEREIN, L. J. 2010 On the scaling and unsteadiness of shock induced separation. Doctoral thesis, Delft University of Technology–Université de Provence.
- SOUVEREIN, L. J. & DEBIÈVE, J. F. 2010 Effects of air jet vortex generators on a shock wave boundary layer interaction. *Experiments in Fluids* **49** (5), 1053–1064.
- SOUVEREIN, L. J., DUPONT, P., DEBIÈVE, J. F., DUSSAUGE, J. P., VAN OUDHEUSDEN, B. W. & SCARANO, F. 2010 Effect of interaction strength on unsteadiness in turbulent shock-wave-induced separations. *AIAA Journal* **48** (7), 1480–1493.
- SOUVEREIN, L. J., VAN OUDHEUSDEN, B. W., SCARANO, F. & DUPONT, P. 2009 Application of a dual-plane particle image velocimetry (dual-PIV) technique for the unsteadiness characterization of a shock wave turbulent boundary layer interaction. *Measurement Science and Technology* **20** (7), 074003 (16pp).
- SPAUD, F. W. & FRISHEIT, J. C. 1972 Incipient separation of a supersonic, turbulent boundary layer, including effect of heat transfer. *AIAA Journal* **10** (7), 915–922.
- SUMMERFIELD, M., FOSTER, C. & SWAN, W. 1954 Flow separation in overexpanded supersonic exhaust nozzles. *Tech. Rep.* Vol. 24. Jet Propulsion Laboratory.
- THOMAS, F. O., PUTMAN, C. M. & CHU, H. C. 1994 On the mechanism of unsteady shock oscillation in shock wave/turbulent boundary layer interaction. *Experiments in Fluids* **18**, 69–81.
- THOMKE, G. J. & ROSHKO, A. 1969 Incipient separation of a turbulent boundary layer at high Reynolds number in two-dimensional supersonic flow over a compression corner. *Tech. Rep.* DAC-59819. NASA Ames Research Center.
- TOUBER, E. & SANDHAM, N.D. 2011 Low-order stochastic modelling of low-frequency motions in reflected shock-wave/boundary-layer interactions. *Journal of Fluid Mechanics* **671** (3), 417–465.
- TOUBER, E. & SANDHAM, N. D. 2008 Oblique shock impinging on a turbulent boundary layer: low-frequency mechanisms. In *38th AIAA Fluid Dynamics Conference, Seattle, Washington, USA*.
- TOUBER, E. & SANDHAM, N. D. 2009a Comparison of three large-eddy simulations of shock-induced turbulent separation bubbles. *Shock Waves* **19** (6), 469–478.
- TOUBER, E. & SANDHAM, N. D. 2009b Large-eddy simulation of low-frequency unsteadiness in a turbulent shock-induced separation bubble. *Theoretical and Computational Fluid Dynamics* **23** (2), 79–107.
- ÜNALMIS, Ö. H. & DOLLING, D. S. 1996 On the possible relationship between low frequency unsteadiness of shock-induced separated flow and Goertler vortices. In *27th AIAA Fluid Dynamics Conference, New Orleans, Louisiana, USA, AIAA-1996-2002*.
- VISWANATH, P. R. 1988 Shock-wave-turbulent-boundary-layer interaction and its control: A survey of recent developments. *Sādhanā* **12**, 45–104.
- WU, M. & MARTIN, M. P. 2008 Analysis of shock motion in shockwave and turbulent boundary layer interaction using direct numerical simulation data. *Journal of Fluid Mechanics* **594**, 71–83.
- ZUKOSKI, E. 1967 Turbulent boundary-layer separation in front of a forward-facing step. *AIAA Journal* **5** (10), 1746–1753.